SCIENCE CHINA
Chemistry

•ARTICLES•

July 2025 Vol.68 No.7: 3260–3267
https://doi.org/10.1007/s11426-025-2724-1

Trimeric carbazole phosphonic acid hole-transporting molecules with robust processability enhance the efficiency of organic solar cells to 20%

Tianqi Chen[1,2†], Yunxin Zhang[1†], Wenkai Zhao[1], Yanyi Zhong[3], Wanying Feng[2], Baofa Lan[1], Xuehang Dong[1], Jingwen Yang[1], Jiangbin Zhang[3,4,5], Kai Han[3,4], Guankui Long[1*], Bin Kan[1*] & Yongsheng Chen[2]

[1]*School of Materials Science and Engineering, National Institute for Advanced Materials, Nankai University, Tianjin 300350, China*
[2]*State Key Laboratory and Institute of Elemento-Organic Chemistry, Frontiers Science Center for New Organic Matter, The Centre of Nanoscale Science and Technology and Key Laboratory of Functional Polymer Materials, Renewable Energy Conversion and Storage Center (RECAST), College of Chemistry, Nankai University, Tianjin 300071, China*
[3]*College of Advanced Interdisciplinary Studies, National University of Defense Technology, Changsha 410073, China*
[4]*Nanhu Laser Laboratory, National University of Defense Technology, Changsha 410073, China*
[5]*Hunan Provincial Key Laboratory of High Energy Laser Technology, National University of Defense Technology, Changsha 410073, China*

Received April 2, 2025; accepted April 21, 2025; published online June 3, 2025

Carbazole-based self-assembled molecules have been widely adopted as hole-transporting layers (HTLs) in high-performance organic solar cells (OSCs). However, their practical implementation has been constrained by their limited concentration in solutions and poor solvent tolerance. Herein, to address these limitations, we designed two novel trimeric molecules (TPACz-1 and TPACz-2) that synergistically integrate the structural merits of small molecules with the processing advantages of polymers. Notably, TPACz-2 showed exceptional hole-transporting capacity with uniform coverage on indium tin oxide (ITO) substrates, coupled with robust processability characterized by an extended concentration tolerance range (0.2–1.0 mg mL^{-1}) and compatibility with a broad range of solvents. Binary OSCs based on TPACz-2 showed an excellent power conversion efficiency (PCE) of 19.65% with a short-circuit current density of 27.49 mA cm^{-2} and a fill factor of 80.9%. At the same time, the corresponding ternary devices exhibited a high PCE exceeding 20%. Furthermore, the TPACz-based devices demonstrated superior ambient stability, retaining ~80% of their initial PCE after 680 h at 25% relative humidity, substantially outperforming conventional PEDOT:PSS-based counterparts. This work offers valuable guidance and highlights the crucial role of oligomeric molecular design as a pivotal strategy for the development of innovative HTLs in OSCs.

organic solar cell, hole-transporting layer, trimeric materials, self-assembled molecules, power conversion efficiency

Citation: Chen T, Zhang Y, Zhao W, Zhong Y, Feng W, Lan B, Dong X, Yang J, Zhang J, Han K, Long G, Kan B, Chen Y. Trimeric carbazole phosphonic acid hole-transporting molecules with robust processability enhance the efficiency of organic solar cells to 20%. *Sci China Chem*, 2025, 68: 3260–3267, https://doi.org/10.1007/s11426-025-2724-1

1 Introduction

Organic solar cells (OSCs) have attracted significant attention as a next-generation photovoltaic technology owing to their solution processability, flexibility, lightweight nature, and compatibility with large-area printing [1–5]. To date, considerable advancements have been made in OSCs because of the development of new device fabrication techniques and materials [6], particularly non-fullerene acceptors

†Equally contributed to this work.
*Corresponding authors (email: longgk@nankai.edu.cn; kanbin04@nankai.edu.cn)

[7,8], with the best verified power conversion efficiency (PCE) of 20.43% for single-junction cells [9]. Notably, the performance of OSCs depends not only on the intrinsic properties of the active materials but also on the interface between the electrode and active layers [1,10,11]. In the conventional manufacturing of sandwich-structure OSCs, the key step is the coating of two charge-transport materials under/onto the active layers via spinning or vacuum evaporation, which is imperative to facilitate charge transport or extraction [12,13]. Poly(3,4-ethylenedioxythiophene):poly (styrene sulfonate) (PEDOT:PSS) is a widely used hole-transporting layer (HTL) material between the photoactive layer and the anode in OSCs because of its efficient hole collection capability and solution processability [14–16]. However, its inherent acidity and hygroscopic nature compromise the long-term stability of devices [14,17–20].

As an alternative strategy, carbazole-based self-assembled molecules are amphiphilic organic compounds exhibiting electron localization and hole selection when coated as a monolayer on indium tin oxide (ITO) electrodes (anchored via the terminal phosphonic acid group), modulating the wettability or adhesion and improving the efficiency and stability of OSCs [17,21–25]. Following the use of 2-(9*H*-carbazol-9-yl)ethyl)phosphonic acid (2PACz) as a HTL material to modify ITO electrodes in OSCs, a series of halogenated 2PACz derivatives and other types of self-assembled molecules have been developed to optimize interfacial layers, thereby enhancing the performance of OSCs [26–30]. Ge *et al*. [31] developed two benzocarbazole-based molecules with a monophosphate group as HTLs, with corresponding binary devices based on PM6:BTP-eC9 attaining a record PCE of 19.7%. Liu *et al*. [32] designed a diphosphonic acid-based self-assembled molecule 3-BPIC-F, with the corresponding devices showing a high PCE of 19.71% with improved hole extraction and low interfacial impedance.

Generally, most commonly reported self-assembled molecules, while possessing definite structures, exhibit particularly sensitivity to thickness and coverage when employed as hole-transporting materials in OSCs [33]. They may exhibit a tendency for uneven molecular packing and coverage due to the strong aggregation of the planar carbazole backbones [34]. To address these challenges, a polymerization strategy has been proposed [35]. Chen *et al*. [36] synthesized Poly-2PACz through the polymerization of carbazole phosphonic acid, which outperformed 2PACz in terms of thickness tolerance, film uniformity, and conductivity, showing a higher PCE (19.1%) than 2PACz (17.5%). Furthermore, Poly-4PACz (4PACz, 4-(9*H*-carbazol-9-yl)butyl)phosphonic acid) was developed to address the critical issue of limited thickness tolerance, effectively facilitating the fabrication of perovskite modules [37]. However, considering the batch-to-batch variations arising from polymer dispersity, the oligomeric molecule design strategy was adopted to harness the complementary merits of well-defined small molecules and polymeric materials [38–40].

Herein, we synthesized two trimeric hole-transporting materials, ((9′-(4-phosphonobutyl)-[3,3′:6′,3″-tercarbazole]-9,9″-diyl)bis-(butane-4,1-diyl))bis-(phosphonic acid) (TPACz-1) and ((9′-(4-phosphonobutyl)-[3,2′:7′,3″-tercarbazole]-9,9″-diyl)bis-(butane-4,1-diyl))bis-(phosphonic acid) (TPACz-2) (Scheme S1, Supporting Information online), by combining three small carbazole molecules with butyl-phosphonic acid as the anchoring group. TPACz-1 and TPACz-2 demonstrated better conductivity and thickness tolerance compared with their small-molecular counterpart 4PACz. TPACz-1 and TPACz-2 formed uniform films on the ITO surface. Consequently, binary PM6:L8-BO blend devices with TPACz-1 and TPACz-2 as HTLs showed PCEs of 19.02% and 19.65%, respectively, higher than the PCE of the device with PEDOT:PSS (18.90%). Moreover, a PM6:L8-BO:BTP-eC9 ternary device with TPACz-2 exhibited a PCE exceeding 20%, indicating that TPACz-2 is a promising HTL material for high-performance OSCs. Surprisingly, the two trimeric HTLs showed superior thickness tolerance than 4PACz, and TPACz-2 processed from different solvents maintains excellent efficiency, which is favorable for the high-throughput fabrication of OSCs.

2 Results and discussion

The synthesis routes of TPACz-1 and TPACz-2 are shown in Scheme S1 and the corresponding detailed procedures are provided in the Supporting Information. We attempted to grow TPACz-1 and TPACz-2 single crystals for a detailed analysis of their molecular packing. Note that we eliminated phosphate groups from the side chains to mitigate their adverse effect on crystallization behavior. As illustrated in Figure 1a, the TPACz-2 single crystal was successfully obtained and TPACz-1 exhibited poor crystallinity, preventing the formation of a single crystal (CCDC No. 2429741, Figure S1, Supporting Information online). Structural analysis revealed three primary packing modes in TPACz-2 (Figure S2), with its enhanced crystallinity relative to TPACz-1 likely contributing to improved charge transport efficiency through optimized molecular ordering.

The molecular orbital properties and electrostatic potential distributions of the two HTL materials were calculated using density functional theory. TPACz-1 and TPACz-2 showed similar negative-charge regions along conjugated backbones, but TPACz-2 exhibited a higher dipole moment (3.79 D) than TPACz-1 (1.82 D), which is favorable for down-shifting the work function (WF) of ITO and improving hole extraction [32,41]. Ultraviolet photoelectron spectroscopy (UPS, Figure 1b) was employed to investigate the effects of these

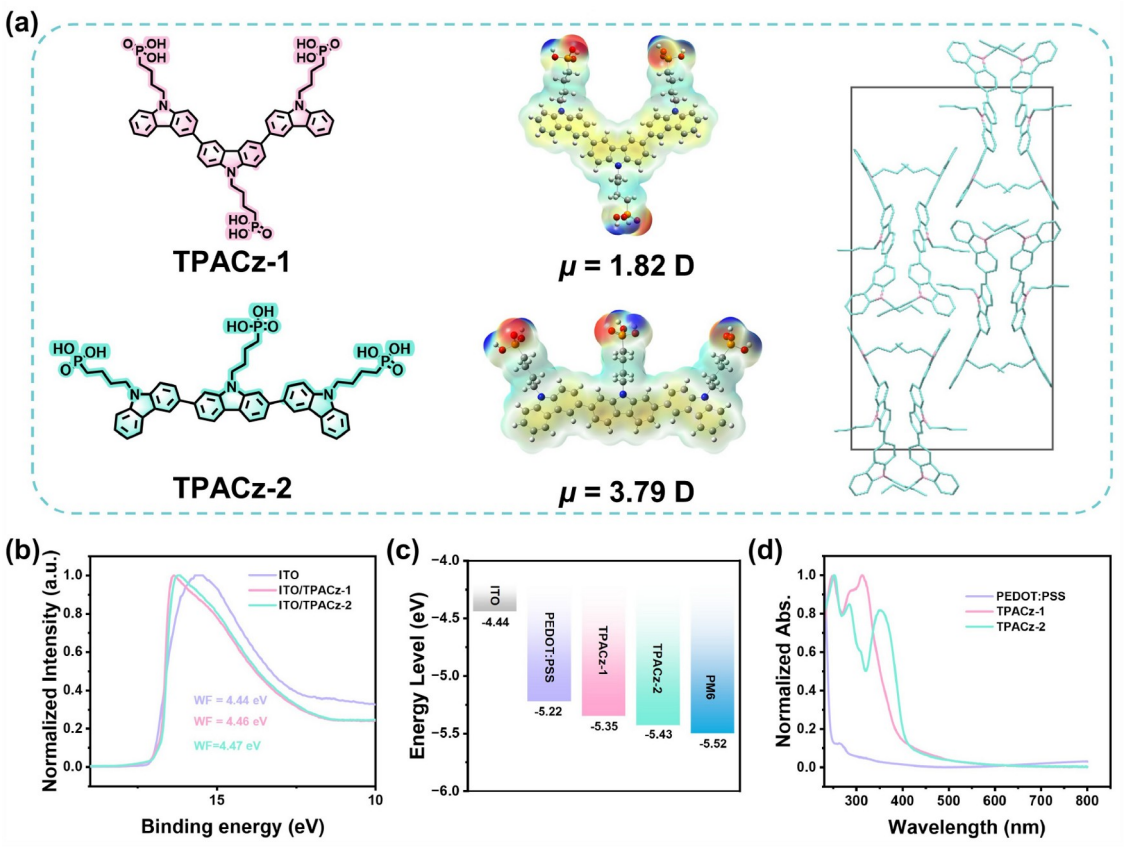

Figure 1 (Color online) (a) Chemical structures of TPACz-1 and TPACz-2 along with their ESP distributions, respectively. Single-crystal packing diagram of TPACz-2 (the phosphate groups were eliminated from the side chains). (b) The UPS of bare ITO, ITO/TPACz-1, and ITO/TPACz-2. (c) The diagram of the energy levels of materials used in devices. (d) The absorption spectra of PEDOT:PSS, TPACz-1, and TPACz-2.

molecules on the WF of ITO. The two designed trimeric HTLs slightly downshifted the Fermi energy level of the ITO substrate, resulting in marginal increases in the WF. As shown in Figure 1c**,** cyclic voltammetry was employed to investigate the highest occupied molecular orbital (HOMO) energy levels of TPACz-1 and TPACz-2 (Figure S3, detailed calculations are provided in Supporting Information online). The lower HOMO energy levels of TPACz-1 and TPACz-2 compared with that of PEDOT:PSS indicated a narrower energy offset with the PM6 donor, implying more effective extraction of holes at the interface between active layers and the anode [42]. The HOMO electron clouds of TPACz-1 and TPACz-2 located on the backbone of carbazole, with their energy levels were calculated at −4.86 and −4.93 eV, consistent with cyclic voltammetry results (Figure S4). As plotted in Figure 1d, although the TPACz-1 and TPACz-2 films showed higher absorption in the ultraviolet-near infrared region than PEDOT:PSS, the spectral contribution to current generation is minimal, resulting in a negligible effect on the device photo-utilization efficiency (detailed discussion follows below).

The effective coverage of hole-collecting materials on the ITO surface is crucial for hole extraction in OSCs. Atomic force microscopy-infrared spectroscopy (AFM-IR) was employed to assess the coverage of TPACz-1 and TPACz-2 using the C–C stretching vibration absorption peak of carbazole in IR absorption spectra (Figure S5). As displayed in the AFM-IR images (Figure 2a, b), TPACz-1 and TPACz-2 exhibited strong IR responses, indicating their uniform distribution on the ITO substrate [32]. Moreover, we used Kelvin probe force microscopy (KPFM) to confirm the uniform coverage of TPACz-1 and TPACz-2 on ITO [34,43]. As shown in Figure 2c, d, the KPFM images indicated subtle variations in the surface potential, implying the uniform dispersion of TPACz-1 and TPACz-2 and thus corroborating the AFM-IR results. Meanwhile, the ITO/TPACz-2 displayed a slightly smoother surface than TPACz-1, favoring charge transport (Figure S6). Notably, the reflectance of the HTL-coated ITO samples was slightly higher than that of pristine ITO, implying almost no detrimental effect of the HTLs on light absorption (Figure S7). Previous studies demonstrated that phosphonic-acid-based carbazole HTLs typically exhibit low interfacial resistance. Herein, the conductivity of HTLs was measured to assess the interfacial resistance of the ITO/HTL/Ag structure. The conductivity of TPACz-2 (1.42×10^{-4} m^{-1}) was higher than those of

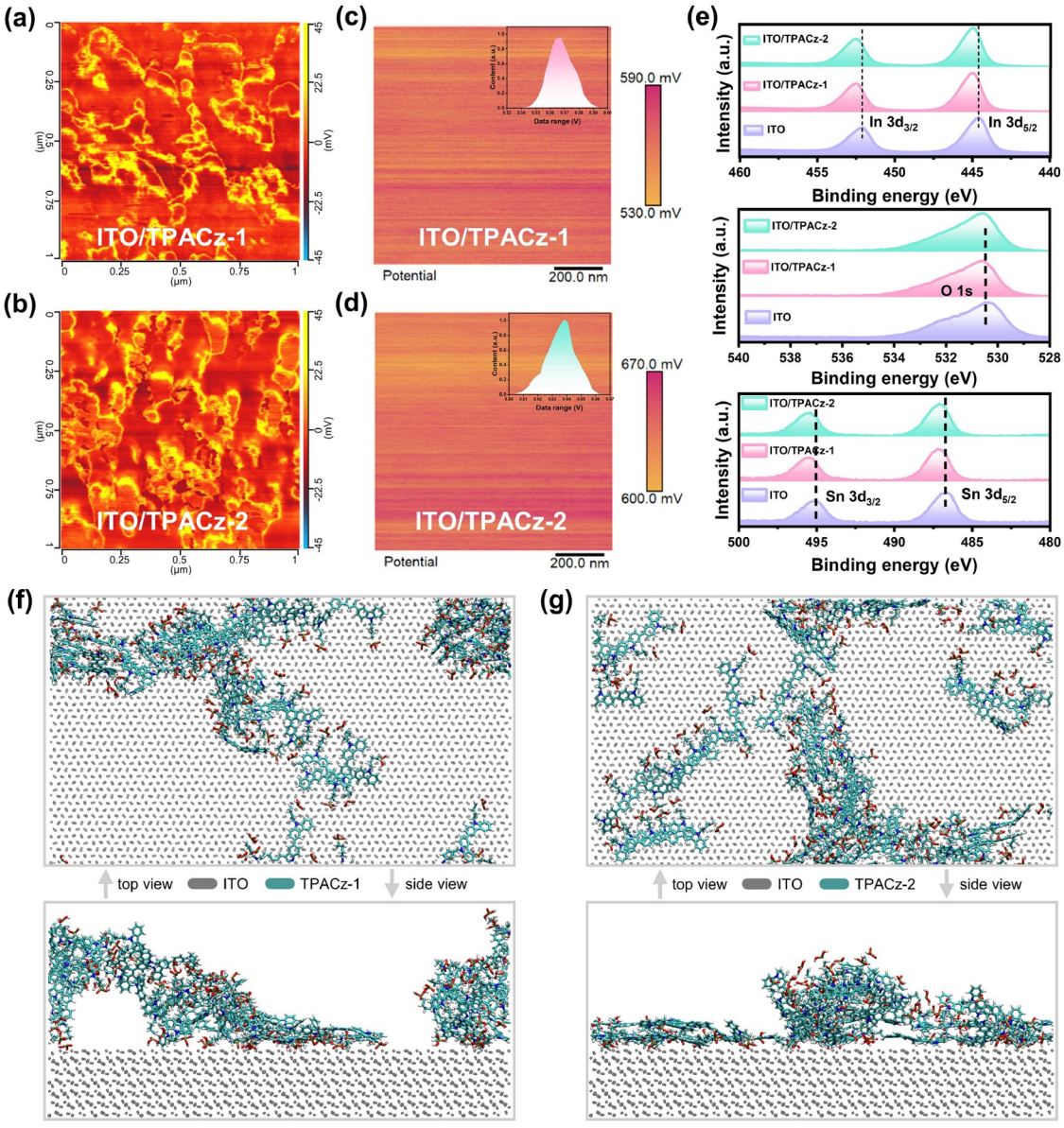

Figure 2 (Color online) AFM-IR images of (a) TPACz-1 and (b) TPACz-2. KPFM images of (c) TPACz-1 and (d) TPACz-2 (inset illustrates the surface potential distribution). (e) In 3d, O 1s, and Sn 3d level XPS spectra of neat ITO, ITO/TPACz-1, and ITO/TPACz-2. Schematic illustration of (f) TPACz-1 and (g) TPACz-2 distribution on an ITO substrate.

TPACz-1 (1.28×10^{-4} m^{-1}) and PEDOT:PSS (0.86×10^{-4} m^{-1}), which is favorable for effective hole extraction (Figure S8 and Table S1, Supporting Information online) [44]. The compatibility between the interface and the electrode/active layer is a pivotal factor that considerably affects the stability and the PCE of OSCs. Therefore, contact angle measurements were performed to investigate the wettability and compatibility of the anode and active blend with TPACz-1/2. The results in Figure S9 reveal the higher contact angle of ITO modified with TPACz HTLs compared to that of bare ITO. Specifically, ITO/TPACz-2 exhibits a higher water contact angle (74.20°) and a smaller glycerol contact angle (70.93°) than ITO/TPACz-1, indicating the better resistance to moisture of the former [31].

The formation of thin self-assembled layers involves the self-organization of molecules via the bonding of the phosphonic acid anchoring group with the metal oxide surface. As illustrated in Figure 2e, X-ray photoelectron spectroscopy of pristine ITO, TPACz-1-coated ITO, and TPACz-2-coated ITO was performed to investigate the chemical interactions between the HTLs and the substrate. A notable shift of the In 3d and Sn 3d peaks is observed after the deposition of TPACz-1 or TPACz-2. The red-shifting of the peaks indicates strong interactions between the trimeric HTLs and ITO, consistent with the results of UPS. To investigate the molecular stacking behavior of two HTLs on ITO substrates,

molecular dynamics (MD) simulations were performed (Figure 2f, g). Detailed computational methods are provided in the Supporting Information online. Molecular dynamics simulations demonstrated that TPACz-2 achieved more uniform molecular alignment and superior substrate coverage (33%) on ITO substrate compared to TPACz-1 (26%), resulting in enhanced hole extraction/transport efficiency (Figure S10). The comparatively inferior film-forming capability of TPACz-1 may originate from its stronger propensity for intermolecular aggregation, which could compromise the formation of homogeneous thin films.

To assess the effect of the two trimeric HTLs on the photovoltaic properties of OSCs, OSCs with an ITO/HTL/PM6:L8-BO/PNDIT-F3N/Ag bulk heterojunction architecture were fabricated and optimized as summarized in Figure S11 and Tables S2–S4. The current density-voltage (*J-V*) curves for the optimized OSCs are presented in Figure 3a, and the photovoltaic parameters are summarized in Table 1. The devices incorporating TPACz-1 and TPACz-2 demonstrate superior short-circuit current density (J_{sc}) of 27.17 and 27.49 mA cm^{-2}, respectively, representing a significant enhancement compared to the PDEOT:PSS-based counterpart (26.83 mA cm^{-2}), which correlates well with their enhanced conductivity results. The device with TPACz-2 shows the highest PCE of 19.65%, along with an open-circuit voltage (V_{oc}) of 0.884 V and a fill factor (FF) of 80.9%, outperforming the conventional cells based on PEDOT:PSS (PCE of 18.90% with the V_{oc} of 0.880 V and FF of 79.8%). The device with TPACz-1 exhibits a slightly lower PCE of 19.02% because of the limited increase in J_{sc}. EQE measurements were used to evaluate the photon response of the cells. The integrated J_{cal} values obtained from the EQE spectra of the devices modified with PEDOT:PSS, TPACz-1, and TPACz-2 are 26.06, 26.33, and 26.58 mA cm^{-2}

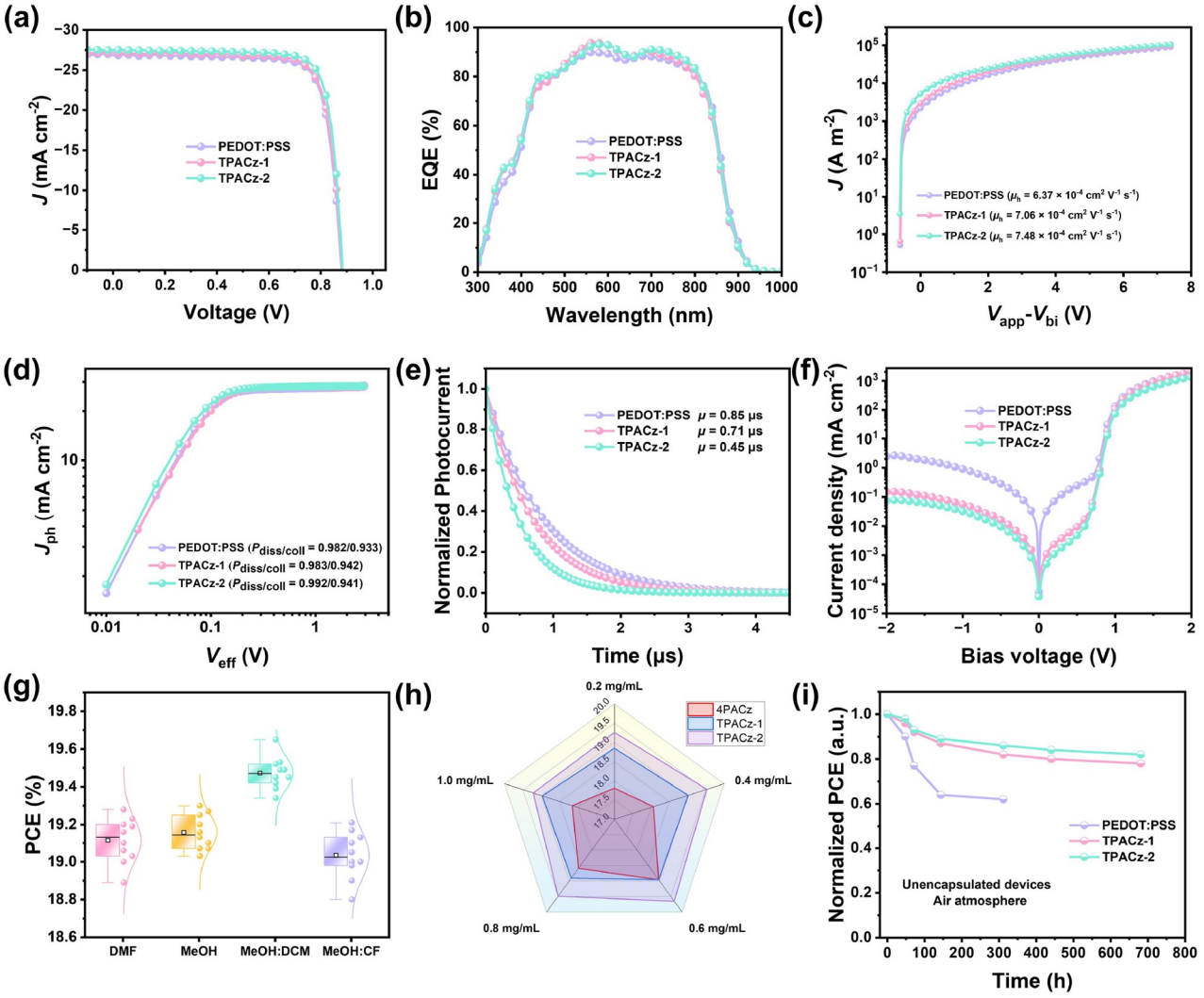

Figure 3 (Color online) (a) *J-V* curves, (b) EQE spectra of the PM6:L8-BO based devices with different HTLs. (c) Hole mobility for devices with the structure of ITO/HTLs/PM6:L8-BO/MoO_3/Ag. (d) Photocurrent density *versus* effective bias characteristics of the corresponding devices. (e) TPC spectra and (f) dark *J-V* curves for different devices. (g) Statistical plots of device PCE for TPACz-2 processed with different solvents. (h) Diagrammatically comparing TPACz-2 across varying concentrations. (i) Air stability of the OSCs based on PEDOT:PSS, TPACz-1, and TPACz-2 HTLs.

Table 1 Photovoltaic parameters of OSCs based on PM6:L8-BO and PM6:L8-BO:BTP-eC9 processed with different HTLs Mix-1 is the solvent of MeOH:DCM and Mix-2 is MeOH:CF. The average values are obtained from 10 individual devices

HTLs	V_{oc} (V)	J_{sc} (mA cm^{-2})	J_{sc}^{cal} (mA cm^{-2})	FF (%)	PCE (%)
PEDOT:PSS	0.880 (0.881±0.007)	26.83 (26.90±0.32)	26.06	79.8 (79.2±0.9)	18.90 (18.80±0.07)
TPACz-1	0.882 (0.882±0.004)	27.17 (27.16±0.22)	26.33	79.4 (79.2±0.8)	19.02 (18.99±0.02)
TPACz-2 (Mix-1)	0.884 (0.880±0.004)	27.49 (27.52±0.21)	26.58	80.9 (80.4±0.5)	19.65 (19.47±0.09)
TPACz-2 (DMF)	0.873 (0.871±0.003)	27.67 (27.50±0.13)	26.68	79.9 (79.7±0.3)	19.28 (19.11±0.12)
TPACz-2 (MeOH)	0.882 (0.880±0.002)	27.39 (27.30±0.17)	26.22	79.9 (79.7±0.2)	19.30 (19.16±0.09)
TPACz-2 (Mix-2)	0.882 (0.883±0.003)	27.36 (27.32±0.23)	26.16	79.7 (79.1±0.6)	19.21 (19.03±0.13)
TPACz-2[a)]	0.872 (0.877±0.003)	28.80 (28.73±0.17)	27.68	79.6 (79.0±0.4)	20.06 (19.93±0.10)

a) The ternary device based on PM6:L8-BO:BTP-eC9 was processed by TPACz-2.

(Figure 3b), respectively, consistent (within 4%) with the J_{sc} values obtained from the *J-V* curves. Furthermore, the TPACz-2-based binary device D18:L8-BO and ternary device PM6:L8-BO:BTP-eC9 achieve a PCE of 19.52% and 20.06%, respectively, underscoring the promise of TPACz-2 for high-performance OSCs (Figures S12 and S13).

The hole mobilities (μ_h) were estimated using the space-charge limited-current method for hole-only devices with the ITO/HTL/PM6:L8-BO/MoO_3/Ag structure in Figure 3c to quantitatively evaluate the effects of TPACz-1 and TPACz-2 on hole transport (electron mobility results are presented for reference in Figure S14). The μ_h of the TPACz-1- and TPACz-2-based devices reach 7.06×10^{-4} and 7.48×10^{-4} cm^2 V^{-1} s^{-1}, respectively, surpassing that of the PEDOT:PSS counterpart, indicating more effective hole transport in the trimeric molecules-modified devices. Additionally, we explored the photon absorption and exciton dissociation processes by determining the relationship between the effective voltage (V_{eff}) and photocurrent density (J_{ph}). As plotted in Figure 3d, the devices with TPACz HTLs show greater P_{diss} than those with PEDOT:PSS, implying more efficient exciton dissociation in the former, thereby resulting in improved J_{sc}. Transient photocurrent measurements were conducted to gain deeper insight into the enhanced J_{sc} of the TPACz-based devices from the perspective of carrier extraction. As shown in Figure 3e, the device with TPACz-2 exhibits ultrafast charge extraction (0.45 μs), outperforming the devices with TPACz-1 (0.71 μs) and PEDOT:PSS (0.85 μs). To further elucidate the origin of the enhanced PCEs of the devices with TPACz-1/2 as HTLs, the *J-V* characteristics of corresponding devices in the dark were obtained (Figure 3f). The devices with TPACz-1/2 exhibit lower leakage current under a reverse bias voltage than the device with PEDOT:PSS, suggesting suppressed electron injection at the anode interface in the former devices, particularly in TPACz-2. These findings align well with the J_{sc} observed for the respective OSCs.

Generally, processing solvents play a vital role in the optimization of the morphology of the active blends, thus affecting the OSC performance. Solvents affect the properties of HTLs, such as PEDOT:PSS; thus, the processability of interfacial materials in a broad range of solvents is an important factor for device fabrication. As shown in Figure 3g and Table 1, the PM6:L8-BO devices with TPACz-2 as the HTL maintain an average PCE of over 19% with different operational solvents, with the best results attained when TPACz-2 was processed using a mixture of methanol and dichloromethane as a solvent (Figure S15). The above results indicate the slight dependence of TPACz-2 on the solvent. Furthermore, a series of HTLs prepared at different concentrations were utilized to fabricate OSC devices. As shown in Figure 3h, trimeric TPACz-1 and TPACz-2 exhibit better concentration tolerance (0.2–1.0 mg mL^{-1}) than small-molecule 4PACz, maintaining PCE variation below 3%. It is well known that the hygroscopic nature of PEDOT:PSS is detrimental to its long-term stability. At the same time, the hydrophilic phosphonic acid groups in TPACz-1 and TPACz-2 bond with ITO, resulting in the exposure of only hydrophobic conjugated carbazole groups, which is beneficial for air stability. As shown in Figure 3i, the target unencapsulated cells with TPACz-1 and TPACz-2 maintained 78% and 82% of their initial PCE (Figure S16), respectively, after 680 h of storage in ambient air, exhibiting better stability than the cell with PEDOT:PSS (62% after 310 h). Furthermore, we fabricated the device with a larger effective area (1 cm^2) using TPACz-2, achieving a PCE exceeding

17% (Figure S17 and Table S7).

To investigate the charge carrier dynamics, we performed transient absorption spectroscopy on the bilayer structures with different HTLs. Figure 4a–c shows the 2D transient absorption spectra of the PEDOT:PSS, TPACz-1, and TPACz-2 bilayers, and the corresponding spectra profiles at different delay times are presented in Figure 4d–f. When excited at 800 nm wavelength, the three samples show ground-state bleaching peaks at 630 and 750 nm, which were assigned to the PM6 donor and L8-BO acceptor, respectively. The prompt signal at 915 nm was ascribed to the photoinduced absorption (PIA) of the L8-BO excitons (Figure S18). The effective exciton dissociation and hole transfer of the three blends are confirmed in Figure S19. The transition of the signal at ~700 nm from negative to positive was attributed to the charge of PM6 or the formation of interfacial charge-transfer (CT) states, indicating that this process is closely related to the formation of free charges. Therefore, we fitted the rising (bi-exponential) and decaying (mono-exponential) parts of this signal to investigate the charge formation and extraction dynamics across the three HTLs. The detailed results are presented in Table S8. The bilayer sample with TPACz-2 exhibits rapid formation and slow decay, suggesting that TPACz-2 plays a pivotal role in enhancing charge generation and extraction. This was attributed to the ability of TPACz-2 to facilitate the formation of an efficient charge-transport channel, consistent with increased J_{sc}.

3 Conclusions

Herein, two isomeric tercarbazole derivatives with three phosphonic acid anchoring groups (TPACz-1 and TPACz-2) were designed and synthesized for use as hole-collecting layers, and TPACz-2 showed excellent hole-transporting capability and broad solution tolerance. Additionally, TPACz-2 exhibited a larger dipole moment, lower surface energy, and stronger interaction with ITO than TPACz-1, resulting in enhanced hole collection capability and reduced interfacial charge recombination in the former. Consequently, OSCs with TPACz-2 achieved a champion PCE of 19.65%, which is higher than that of the device with TPACz-1 (19.02%). Additionally, the binary device D18:L8-BO and ternary device PM6:L8-BO:BTP-eC9 processed by TPACz-2 obtained a PCE of 19.52% and 20.06%, respectively, demonstrating the potential of TPACz-2 in fabricating high-performance devices. Notably, the un-

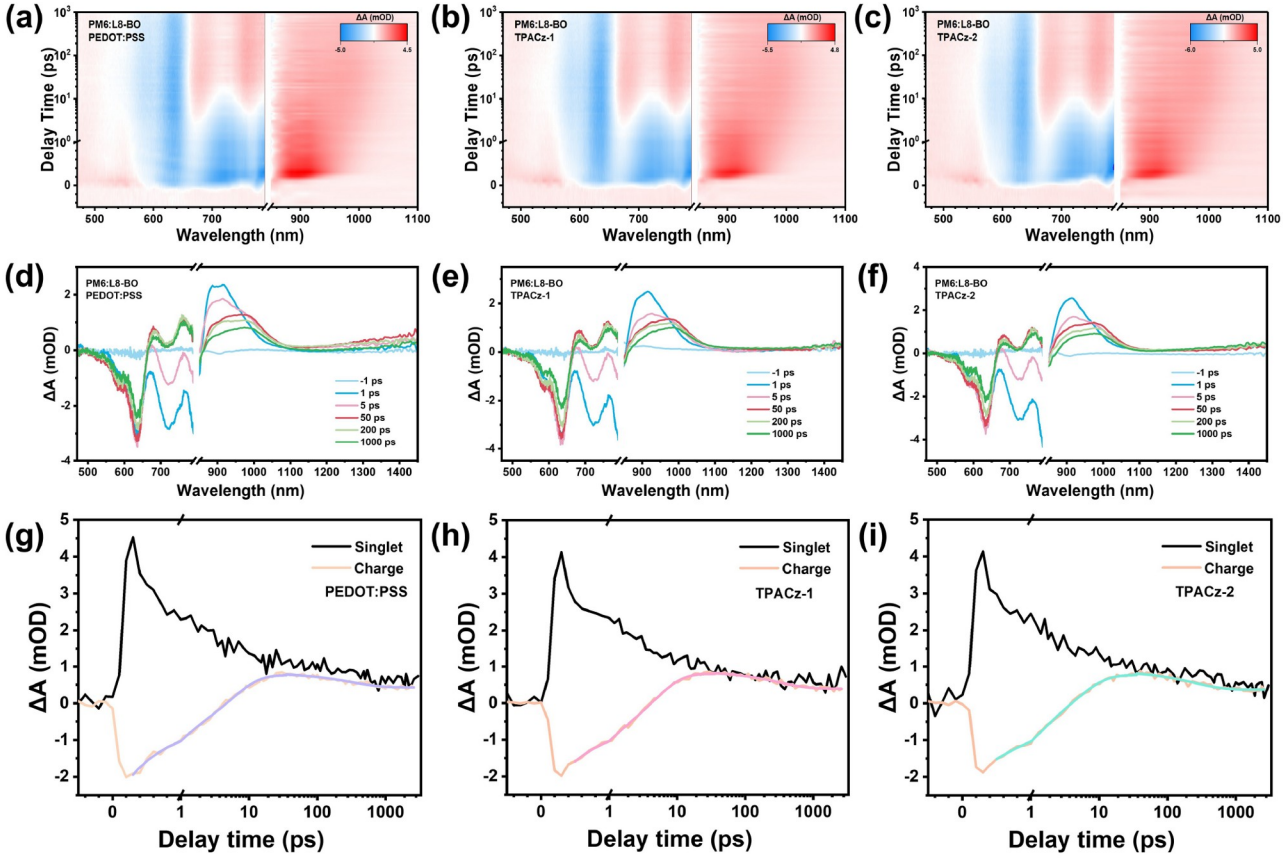

Figure 4 (Color online) 2D transient absorption (TA) spectrum of the bilayer excited at 800 nm in (a) PEDOT:PSS/PM6:L8-BO, (b) TPACz-1/PM6:L8-BO, and (c) TPACz-2/PM6:L8-BO. (d–f) The corresponding TA spectra. Excited state dynamics diagram of blend films based on (g) PEDOT:PSS, (h) TPACz-1, and (i) TPACz-2.

encapsulated TPACz-based devices retain approximately 80% efficiency after 680 h in air (25% relative humidity), indicating their considerably higher air stability than that of the PEDOT:PSS-based device (about 60% after 310 h). Moreover, TPACz-2 exhibited compatibility with a broad range of solvents and low sensitivity to thickness, which is beneficial for the fabrication of OSCs through large-area printing. The above findings indicate that TPACz-2 is a promising HTL material with defined chemical structure and robust processability. The present study serves as a valuable reference for the development of highly efficient and robust hole-transporting materials, ultimately driving the advancement of organic photovoltaic devices.

Acknowledgements This work was supported by the Ministry of Science and Technology of China (2023YFE0210400), the National Natural Science Foundation of China (22361132530, 52303237), the Natural Science Foundation of Tianjin (24JCYBJC01540), and the Fundamental Research Funds for the Central Universities (023-63253172).

Conflict of interest The authors declare no conflict of interest.

Supporting information The supporting information is available online at http://chem.scichina.com and http://link.springer.com/journal/11426. The supporting materials are published as submitted, without typesetting or editing. The responsibility for scientific accuracy and content remains entirely with the authors.

1 Yi J, Zhang G, Yu H, Yan H. *Nat Rev Mater*, 2024, 9: 46–62
2 Li S, Li Z, Wan X, Chen Y. *eScience*, 2023, 3: 100085
3 Zhang G, Lin FR, Qi F, Heumüller T, Distler A, Egelhaaf HJ, Li N, Chow PCY, Brabec CJ, Jen AKY, Yip HL. *Chem Rev*, 2022, 122: 14180–14274
4 Cheng P, Li G, Zhan X, Yang Y. *Nat Photon*, 2018, 12: 131–142
5 Yao H, Ye L, Zhang H, Li S, Zhang S, Hou J. *Chem Rev*, 2016, 116: 7397–7457
6 Zou W, Sun Y, Sun L, Wang X, Gao C, Jiang D, Yu J, Zhang G, Yin H, Yang R, Zhu H, Chen H, Gao K. *Adv Mater*, 2025, 37: 2413125
7 Yuan J, Zhang Y, Zhou L, Zhang G, Yip HL, Lau TK, Lu X, Zhu C, Peng H, Johnson PA, Leclerc M, Cao Y, Ulanski J, Li Y, Zou Y. *Joule*, 2019, 3: 1140–1151
8 Yan C, Barlow S, Wang Z, Yan H, Jen AKY, Marder SR, Zhan X. *Nat Rev Mater*, 2018, 3: 18003
9 Chen H, Huang Y, Zhang R, Mou H, Ding J, Zhou J, Wang Z, Li H, Chen W, Zhu J, Cheng Q, Gu H, Wu X, Zhang T, Wang Y, Zhu H, Xie Z, Gao F, Li Y, Li Y. *Nat Mater*, 2025, 24: 444–453
10 Jiang H, Liang Q, Guo H, Zhang A, Wang X, Tang Z, Bo Z. *J Am Chem Soc*, 2024, 146: 30262–30271
11 Braun S, Salaneck WR, Fahlman M. *Adv Mater*, 2009, 21: 1450–1472
12 Chen Z, Li Q, Tang H, Wen J, Zhong Y, Zhang J, Han K, Liu Y. *Angew Chem Int Ed*, 2025, 64: e202424502
13 Zhang X, Tang Q, Yao X, Chen Q, Zhang ZG, Shen P, Weng C. *Nano Energy*, 2025, 137: 110799
14 Jiang Y, Dong X, Sun L, Liu T, Qin F, Xie C, Jiang P, Hu L, Lu X, Zhou X, Meng W, Li N, Brabec CJ, Zhou Y. *Nat Energy*, 2022, 7: 352–359
15 Zheng Z, Hu Q, Zhang S, Zhang D, Wang J, Xie S, Wang R, Qin Y, Li W, Hong L, Liang N, Liu F, Zhang Y, Wei Z, Tang Z, Russell TP, Hou J, Zhou H. *Adv Mater*, 2018, 30: 1801801
16 Zeng M, Wang X, Ma R, Zhu W, Li Y, Chen Z, Zhou J, Li W, Liu T, He Z, Yan H, Huang F, Cao Y. *Adv Energy Mater*, 2020, 10: 2000743
17 Sun X, Ding X, Wang F, Lv J, Gao C, Zhang G, Ouyang X, Li G, Hu H. *ACS Energy Lett*, 2024, 9: 4209–4217
18 Xia Y, Sun K, Ouyang J. *Adv Mater*, 2012, 24: 2436–2440
19 Guan S, Li Y, Xu C, Yin N, Xu C, Wang C, Wang M, Xu Y, Chen Q, Wang D, Zuo L, Chen H. *Adv Mater*, 2024, 36: 2400342
20 Zhao B, Chung S, Zhang M, Wei W, Zhu C, Deng C, Cho K, Kan Z. *Adv Funct Mater*, 2024, 34: 2309832
21 Li Y, Jia Z, Huang P, Liu T, Hu D, Li Y, Liu H, Lu X, Lu S, Yin X, Yang YM. *Adv Energy Mater*, 2024, 14: 2304000
22 Li M, Liu M, Qi F, Lin FR, Jen AKY. *Chem Rev*, 2024, 124: 2138–2204
23 Tang H, Shen Z, Shen Y, Yan G, Wang Y, Han Q, Han L. *Science*, 2024, 383: 1236–1240
24 Li H, Li Y, Dai X, Xu X, Peng Q. *Angew Chem Int Ed*, 2025, 64: e202416866
25 Xu H, Sharma A, Han J, Kirk BP, Alghamdi AR, Xu F, Zhang Y, Emwas A, Hizalan G, De Wolf S, Andersson MR, Andersson GG, Baran D. *Adv Energy Mater*, 2024, 14: 2401262
26 Lin Y, Firdaus Y, Isikgor FH, Nugraha MI, Yengel E, Harrison GT, Hallani R, El-Labban A, Faber H, Ma C, Zheng X, Subbiah A, Howells CT, Bakr OM, McCulloch I, Wolf SD, Tsetseris L, Anthopoulos TD. *ACS Energy Lett*, 2020, 5: 2935–2944
27 Lin Y, Zhang Y, Zhang J, Marcinskas M, Malinauskas T, Magomedov A, Nugraha MI, Kaltsas D, Naphade DR, Harrison GT, El-Labban A, Barlow S, De Wolf S, Wang E, McCulloch I, Tsetseris L, Getautis V, Marder SR, Anthopoulos TD. *Adv Energy Mater*, 2022, 12: 2202503
28 Lin Y, Magomedov A, Firdaus Y, Kaltsas D, El-Labban A, Faber H, Naphade DR, Yengel E, Zheng X, Yarali E, Chaturvedi N, Loganathan K, Gkeka D, AlShammari SH, Bakr OM, Laquai F, Tsetseris L, Getautis V, Anthopoulos TD. *ChemSusChem*, 2021, 14: 3569–3578
29 Gao S, Peng R, Qiu Y, Liu H, Wu Y, Li X, Zhang Y, Jin F, Ge Z. *Adv Funct Mater*, 2025, 35: 2418223
30 Chen Z, Li X, Qin S, Gong Y, Liu Z, Yuan M, Liang TL, Meng L, Li Y. *CCS Chem*, 2025, 7: 507–518
31 Yu X, Ding P, Yang D, Yan P, Wang H, Yang S, Wu J, Wang Z, Sun H, Chen Z, Xie L, Ge Z. *Angew Chem Int Ed*, 2024, 63: e202401518
32 Liu H, Xin Y, Suo Z, Yang L, Zou Y, Cao X, Hu Z, Kan B, Wan X, Liu Y, Chen Y. *J Am Chem Soc*, 2024, 146: 14287–14296
33 Bin H, Datta K, Wang J, van der Pol TPA, Li J, Wienk MM, Janssen RAJ. *ACS Appl Mater Interfaces*, 2022, 14: 16497–16504
34 Yu S, Xiong Z, Zhou H, Zhang Q, Wang Z, Ma F, Qu Z, Zhao Y, Chu X, Zhang X, You J. *Science*, 2023, 382: 1399–1404
35 Wang F, Liu T, Liu Y, Zhou Y, Dong X, Zhang Y, Shi X, Dou Y, Ren Z, Wang L, Zhao Y, Luo S, Hu X, Peng X, Bao C, Wang W, Wang J, Hu W, Chen S. *Adv Mater*, 2024, 36: 2412059
36 Ren Z, Luo S, Shi X, Dou Y, Liu T, Wang L, Tsang KK, Wang F, Zhao Y, Liu Y, Hu X, Peng X, Liu W, Yan H, Chen S. *Sci China Chem*, 2024, 67: 1941–1945
37 Ren Z, Cui Z, Shi X, Wang L, Dou Y, Wang F, Lin H, Yan H, Chen S. *Joule*, 2023, 7: 2894–2904
38 Liu C, Lian Y, Song J, Liu J, Bi Z, Ma W, Sun Y. *Adv Funct Mater*, 2025, 35: 2417786
39 Lee JW, Park JS, Jeon H, Lee S, Jeong D, Lee C, Kim YH, Kim BJ. *Chem Soc Rev*, 2024, 53: 4674–4706
40 Qi F, Li Y, Lin FR, Jen AK. *ChemSusChem*, 2024, 17: e202301559
41 Jeong S, Oh J, Park J, Cho Y, Jung S, Lee S, Park J, Yang C. *ACS Energy Lett*, 2024, 9: 3771–3779
42 Liu L, Yu F, Hu D, Jiang X, Huang P, Li Y, Tian G, Lei H, Wu S, Tu K, Chen C, Gu T, Chen Y, Duan T, Xiao Z. *Energy Environ Sci*, 2025, 18: 1722–1731
43 Li D, Lian Q, Du T, Ma R, Liu H, Liang Q, Han Y, Mi G, Peng O, Zhang G, Peng W, Xu B, Lu X, Liu K, Yin J, Ren Z, Li G, Cheng C. *Nat Commun*, 2024, 15: 7605
44 Chen Z, Zhang S, Zhang T, Dai J, Yu Y, Li H, Hao X, Hou J. *Joule*, 2024, 8: 1723–1734